Tectonic Controls on Nearshore Sediment Accumulation and Submarine Canyon Morphology Offshore La Jolla, Southern California

Nicolas Le Dantec [a, *], Leah J. Hogarth [a], Neal W. Driscoll, [a] and Jeffrey M. Babcock [a]

[a] Scripps Institution of Oceanography, UCSD, 9500 Gilman Drive, La Jolla, CA 92093-0208, USA

Walter A. Barnhardt [b] and William C. Schwab [b]

[b] U.S. Geological Survey, Woods Hole, MA 02543

(Email addresses: nledantec@ucsd.edu, lhogarth@ucsd.edu, ndriscoll@ucsd.edu, jbabcock@ucsd.edu. wbarnhardt@usgs.gov, bschwab@usgs.gov)

* Corresponding author: Last name Le Dantec, First name Nicolas, Tel. (1) 858 822 4312, Fax (1) 858 534 7641, Email address nledantec@ucsd.edu

Abstract

CHIRP seismic and swath bathymetry data acquired offshore La Jolla, California provide an unprecedented three-dimensional view of the La Jolla and Scripps submarine canyons. Shore-parallel patterns of tectonic deformation appear to control nearshore sediment thickness and distribution around the canyons. These shore-parallel patterns allow the impact of local tectonic deformation to be separated from the influence of eustatic sea-level fluctuations. Based on stratal geometry and acoustic character, we identify a prominent angular unconformity inferred to be the transgressive surface and three sedimentary sequences: an acoustically laminated estuarine unit deposited during early transgression, an infilling or “healing-phase” unit formed during the transgression, and an upper transparent unit. Beneath the transgressive surface, steeply dipping reflectors with several dip reversals record faulting and folding along the La Jolla margin. Scripps Canyon is located at the crest of an antiform, where the rocks are fractured and more susceptible to erosion. La Jolla Canyon is located along the northern strand of the Rose Canyon Fault Zone, which separates Cretaceous lithified rocks to the south from poorly cemented Eocene sands and gravels to the north. Isopach and structure contour maps of the three sedimentary units reveal how their thicknesses and spatial distributions relate to regional tectonic deformation. For example, the estuarine unit is predominantly deposited along the edges of the canyons in paleotopographic lows that may have been inlets along barrier beaches during the Holocene sea-level rise. The distribution of the infilling unit is controlled by pre-existing relief that records tectonic deformation and erosional processes. The thickness and distribution of the upper transparent unit is controlled by long-wavelength, tectonically-induced relief on the transgressive surface and hydrodynamics.

Keywords:

Tectonic deformation, Submarine canyon morphology, Nearshore sediment accumulation

1. Introduction

The importance of underlying structures in controlling the formation and evolution of morphological features and sediment accumulation has long been appreciated (Emery, 1958; Shepard and Emery, 1941). Several studies illustrate the influence of tectonic deformation on geomorphology, such as continental slope morphology on tectonically active margins (Pratson and Haxby, 1996) or drainage patterns and formation of fluvial terraces (Peters and van Balen, 2007). Long-term retreat of modern beaches (Honeycutt and Krantz, 2003), the preservation and evolution of barrier-island systems (Belknap and Kraft, 1985; Harris et al., 2005; Schwab et al., 2000; Thieler et al., 2001), and short-term dynamic processes such as the position and stability of sandbars in the nearshore (McNinch, 2004), are also affected by underlying structures. Here we present new geophysical and geological data that show the importance of tectonic deformation in controlling canyon location and morphology and modern sediment distribution offshore La Jolla, California.

The sedimentary and morphological evolution of continental margins depends on many factors, three of which are eustasy, sediment supply, and tectonic deformation (Christie-Blick and Driscoll, 1995; Posamentier and Allen, 1999). Discerning how these parameters affect sediment accumulation is often difficult even when the factors are operating at different spatial scales (Sommerfield and Lee, 2003, 2004). On active margins tectonics play a large role in controlling the nearshore physiography. In our study site, the shore-parallel deformation caused by transpression and transtension associated with the dextral Rose Canyon Fault (Figure 1) can be isolated from the cross-shore oriented base-level changes imparted by regional tectonic uplift and eustatic sea-level fluctuations. Our work examines how local deformation affects the relief on the transgressive surface, which in turn, plays an important role in controlling regions of sediment bypass and accumulation.

The Rose Canyon Fault Zone (RCFZ; Moore, 1972; Treiman, 1993), a right-lateral, strike-slip fault system in the California Borderlands, is a major tectonic feature in the area. Although long assumed to continue offshore beneath the Pacific Ocean from its onshore expression in La Jolla, the first map of the offshore location of the feature was made by Moore (1972) using subbottom profiling. The acoustic reflection profiles imaged the fault for ~60 km to the northwest, but did not resolve its finer scale morphology, especially in the area of the La Jolla submarine canyon. Treiman (1993) combined subbottom profiles and land-based maps to refine the geometry of the RCFZ from San Diego Bay north to Oceanside. His focus was on Holocene seismicity, determining a slip rate of at least 1.0 mm/yr (Treiman, 1993). Transpression has occurred around westward jogs on the fault and created localized areas of uplift, two of which are expressed in the topography of Mount Soledad and the bathymetry and subbottom structure offshore of Torrey Pines State Park (pop-up structure of Hogarth et al., 2007; Figure 1). Wave-cut notches are observed along the shelf at various water depths and appear to record still-stands during the last sea-level rise (Byrd et al., 1975; Darigo and Osbourne, 1986; Emery, 1958; Henry, 1976; Waggoner, 1979).

La Jolla Bay is located at the southern end of the Oceanside littoral cell, which is delineated by Mount Soledad (Figure 1). In this region, sediment transport is predominantly to the south (Inman and Chamberlain, 1960). Multiple studies have examined the Holocene sediment distribution (Henry, 1976; Waggoner, 1979), origin, age, transport mechanisms, and transport pathways (Everts and Dill, 1988; Haas, 2005; Young and Ashford, 2006), particularly in relation to the dynamics of littoral cells (Inman and Masters, 1991a, 1991b). Research on the Quaternary sediment cover on the shelf off San Diego County has also focused on coastal management, protection of marine habitats, and resource inventory for mining purposes (Darigo and Osbourne, 1986). The sediment thickness exhibits a wedge-shaped cross-shore profile with a mid-shelf depocenter (Byrd et al., 1975; Henry, 1976; Hogarth et al., 2007). Sediment input mostly consists of sand and silt derived from river discharge to the north and widespread cliff erosion (Haas, 2005; Stow and Chang, 1987; Young and Ashford, 2006).

Previous work on La Jolla Canyon has yielded fundamental scientific advances in the understanding of canyon morphology and architecture (Buffington, 1964; Shepard and Dill, 1966), the role of canyons for transport between deep oceans and shallow waters, submarine fan stratigraphy (Covault et al., 2007), turbidity flows and bottom canyon currents (Inman et al., 1976), erosive processes accompanying the formation and persistence of canyons (Shepard, 1981), sedimentation and erosion at canyon heads (Chamberlain, 1964; Dill, 1964), and interactions between canyons and biota (Vetter, 1994). The canyon has two branches, the Scripps Branch and the La Jolla Branch. Because the entire canyon has been termed the La Jolla Canyon, for clarity purposes, we will refer to the entire canyon as the La Jolla Canyon System. The La Jolla and Scripps canyon heads extend into shallow water (~8-10 m) and as such they modify nearshore circulation, surface wave patterns, and littoral sediment transport (Shepard and Inman, 1950; Thomson et al., 2005). In addition, currents measured along the floor of the canyons show a strong tidal component (Inman et al., 1976; Shepard et al., 1977).

In this study, high-resolution seismic and bathymetric data acquired offshore La Jolla, California between the surf zone and the shelf break (Figure 2) allow us to examine the tectonic control on the locations of the La Jolla and Scripps submarine canyons as well as the impact of tectonics on postglacial sedimentation on the inner shelf offshore La Jolla. We will first present the results for the canyon morphology and then we will discuss the stratigraphic packages observed along the margin from oldest to youngest based on the first comprehensive maps of their aerial distribution.

2. Methodology

2.1 Data Acquisition

In 2002 and 2003, high-resolution swath bathymetry and seismic data were acquired offshore La Jolla, Southern California during three cruises. The surveys covered the narrow shelf from Point La Jolla north to Penasquitos Lagoon. The survey tracks mostly consist of strike lines with about 150-m line spacing, augmented with four dip lines (Figure 2). We used a SwathPlus-L (formerly Submetrix) interferometric swath bathymetric sonar by SEA Ltd (http://www.sea.co.uk) and the Scripps subbottom reflection sonar system (SUBSCAN), which is a modified EdgeTech (http://www.edgetech.com/) CHIRP system that consists of a dual-transducer X-Star sonar with an ADSL link from the towfish to the topside computers.

The SwathPlus-L sonar, which operates at 117 kHz and has a nominal cross-track resolution up to 15 cm, yielded better than 50-cm horizontal resolution even over the steep topographic features of the survey area, up to at least 75 m depth. The SUBSCAN sonar uses a 50 ms swept pulse across a 1.5 to 5 kHz range with 24° beam width, yielding sub-meter vertical resolution to sub-seafloor depths of approximately 50 m. During the nearshore surveys in 2002 onboard the RV Saikhon, the SwathPlus-L system was attached to a side-mount while the SUBSCAN system was 'floated' on a surface tow frame. The deployment configuration was complemented with an on-board motion sensor and a global positioning system (GPS) receiver to measure attitude and position. Navigation for the seismic data was measured using a second GPS receiver mounted on the surface tow frame. During the offshore survey in 2003 onboard the R/V Sproul, only seismic data were collected and the SUBSCAN system was towed at approximately 10 m above the seafloor. Winch cable payout records were used to correct layback offsets during post-processing. Data were acquired at a ship speed of approximately 4–5 knots during both surveys.

During a scuba dive on Dec 14th 2007, a short push core was acquired from a layer that outcrops along a ridge at 23 meters water depth near the head of La Jolla Canyon (Figures 2 and 3B). The site was selected to ground-truth one of the stratigraphic packages identified in the seismic data, which has a laminated acoustic character and outcrops in this area. A 2-inch diameter clear plastic tube with a tapered extremity was pushed into the seafloor and capped before pulling it out to create suction and improve sediment recovery. The lower end of the core was capped underwater so that the sample was well preserved. The core was split, described and photographed. Other vibracores referenced in relation to geophysical interpretations were collected and processed by Hogarth et al. (2007) and by Darigo and Osborne (1986).

2.2 Data Processing

Processing the raw bathymetry data involved numerous steps. The soundings were corrected incorporating the acquisition parameters - attitude and position - as well as water level fluctuations with the tides using observations from the NOAA tide gauge installed at the Scripps Pier. The vertical datum was shifted from MLLW to NAVD 88. The sound speed in water was adjusted using CTD data, which were collected during the survey to account for density variations between nearshore, shelf, and deeper waters within the submarine canyons. The data volume was gridded at 50-cm resolution with a continuous curvature spline in tension. Finally, the data were smoothed using a linear convolution filter of 11.5 meters averaging window size in both horizontal directions.

The seismic data were converted into standard SEG-Y, heave-corrected, processed, and plotted using SIOSEIS (Henkart, 2003) and SeismicUnix (Cohen and Stockwell, 2002) seismic processing software. In addition, depths to various acoustic reflectors identified in each profile were digitized. The corresponding horizons were then gridded at 10-m resolution and used to generate isopach maps of the stratigraphic packages. In order to convert travel time to sediment thickness, a velocity of 1720 m/s was used for non-silty sediments and a velocity of 1520 m/s was used for water and mud-dominated sediments (Jackson et al., 1996; Buckingham and Richardson, 2002; Williams et al., 2002). We used the software Fledermaus by Interactive Visualization Systems (IVS

3D, http://www.ivs3d.com) to merge all graphic elements into three-dimensional perspective views of the seafloor and subbottom.

3. Results

3.1 Bathymetry

3.1.1 Canyon Morphology

The two canyons, as revealed by high-resolution bathymetry, exhibit very different morphologies (Figure 3). La Jolla Canyon is much wider than Scripps Canyon, especially near its head. Scripps Canyon is ~150 m wide at its seaward extent, but narrows to ~30 m wide near its head. In contrast, the width of La Jolla Canyon is ~250 m along its length, and widens to nearly 500 m at its shoreward extent where incisions form a bowl-shaped head. In addition, Scripps Canyon is very linear, whereas La Jolla Canyon curves gently to the north with a 30° change in its azimuth from the canyon head to where it intersects Scripps Canyon. The Scripps Canyon head is narrow and steep-walled. Conversely, the La Jolla Canyon head is characterized by a concave upwards morphology with moderate slopes. The upper reaches of La Jolla Canyon are dissected by a number of ridges and gullies (Figure 3). Some of these ridges extend quite far into the canyon acting as promontories separating the bowl-shaped canyon heads.

3.1.2 Side Canyons

The morphology of side canyons incised into the walls of the two canyons is also dissimilar. For example, a few large side canyons have incised the margins of La Jolla Canyon deeply enough to intersect consolidated basement rocks. Near or within the head of the canyon, these channels are long and remarkably tortuous, with one in particular taking two well defined and opposite turns ("S"; Figure 3). The incision located on the northern wall of La Jolla Canyon, south of the intersection with Scripps Canyon is wide and rounded, resembling the scalloping on the shelf edge north of Scripps Canyon ("I"; Figure 3). The northern most incision observed in Figure 3 causes a shoreward inflexion of the 75 m isobath, that appears as a depression in the bathymetry (northern most "I"; Figure 3A). In contrast with La Jolla Canyon, the side canyons of Scripps Canyon are shallower, smoother-walled, and are primarily incised into unconsolidated sediments. Side canyons have generally incised oblique to the axis of Scripps Canyon, and some extend far away from its axis (~500 m, Figure 3) despite their gentle slopes. Farther north along the margin, a structure resembling a side canyon is observed in the bathymetry, which defines the southeast corner of the pop-up structure and is where the Rose Canyon Fault takes a westerly jog (Figure 1).

3.1.3 Asymmetry between the north and south walls

The canyon walls exhibit marked asymmetry (Figure 3). For example, most of the ridges and side canyons of La Jolla Canyon occur on its north wall. Conversely, the south wall has few or no secondary incisions, especially in the shallow section near the canyon head. In Scripps Canyon, secondary incisions are more frequent, larger, and deeper along the south wall. Despite these differences, the canyons also share some morphologic features. One similarity is the northward orientation of their heads. As the canyons trend shoreward across the shelf, their shallow-water extensions are preferentially developed towards the north. Another common trait is that, except for the head of La Jolla Canyon, the slopes of the walls are very steep in both canyons.

3.2 Regional Angular Unconformity

A regional angular unconformity is identified in seismic profiles and mapped throughout the study area. The surface is typically identified by dipping and truncated reflectors below (Figure 4) and is overlain by relatively flat-lying reflectors or an acoustically transparent unit (Figure 5). Regionally, the bedding beneath the angular unconformity dips to the south, but three areas exhibit reversals in this trend (Figure 4). The major regions where bedding dips to the north are the following: 1) directly north of La Jolla Canyon, 2) directly north of Scripps Canyon, and 3) in the localized offshore high aligned with the Carmel Valley Fault (Figure 4). Where the reversal of dip is observed offshore, the units dip more steeply to the north (~15-20°) than those measured onshore (~5-10°; Kennedy, 1975).

In areas where the unconformity was difficult to identify based on stratal geometry, it was traced laterally from regions where it could be confidently identified. Deposition above the angular unconformity exhibits much variability ranging from acoustically laminated onlapping deposits to acoustically transparent deposits (Figure 5). In some areas the angular unconformity becomes the seafloor (Figures 6 and 7B). Hogarth et al. (2007) identified this unconformity as the transgressive surface from the last deglaciation (~21 ka to present). Throughout much of the study area, the transgressive surface coalesces with the underlying sequence boundary formed during the last sea-level fall (~120 to 21 ka), but the two surfaces appear to diverge in the canyon regions.

The transgressive surface shows much variability in topography and roughness in the along-shore and cross-shore directions. It has relatively high relief on either side and in the immediate proximity of the La Jolla and Scripps canyons. To the south of La Jolla Canyon, the transgressive surface shallows where Cretaceous mudstones outcrop on the seafloor. Between the two canyons the transgressive surface is relatively flat, uniformly slopes to the northwest, and is overlain by up to 20 m of sediments. The high in the transgressive surface near Scripps Canyon is more pronounced to the north of the canyon (Figures 7A, 8, and 9B). A constraining bend in the Rose Canyon Fault creates a structural high in the transgressive surface in the northern portion of our study area. A saddle along the transgressive surface is observed between the high coincident with Scripps Canyon and the high associated with the pop-up structure (Figures 5, 8, and 9B). Within this low, strike profiles show a localized high offshore with an along- and cross-shore extent of ~1 km and moderate vertical relief of a few meters (Figure 5). Dip lines show several notches or wave-cut terraces on the transgressive surface that have relief on the order of several meters (Figure 7B).

A notable decrease in roughness along the transgressive surface is observed from offshore to onshore (Figure 5). The onshore trends of the Carmel Valley, Salk, and Torrey Pines faults appear to be aligned with the deformation observed in water depths > ~45 m (Figures 2, 4, and 5). At shallower depths, the expression of the fault on the transgressive surface is subtle and only delineated by changes in bedding orientation below the transgressive surface. Furthermore, wave-cut terraces on the transgressive surface are confined to water depths > 20-30 m and their relief increases with depth (Figure 7B).

Observations from the sea cliffs in our survey area offer an ideal opportunity to examine the along-shore variability of the tectonic landscape, which complements our offshore observations. In the northern part of our study area, Legg and Kennedy (1979) identified a system of east-west trending oblique faults, including the Carmel Valley and Salk faults. Sea cliffs between the south extremity of La Jolla Shores beach and Point La Jolla are of particular significance because they lie within the RCFZ, where trench studies suggest Holocene deformation (Lindvall and Rockwell, 1995). Along the seacliffs, we observe three strike-slip faults, namely the Country Club, Mount Soledad, and Rose Canyon faults from south to north (Figure 2; Treiman, 1993), as well as a number of more diffuse fault splays. The change in coastal relief from the low-lying La Jolla Shores to the uplifted and deformed sea cliffs along Mount Soledad parallels the change in seabed type from sandy bottom to the kelp-bearing rocky substrate observed around Point La Jolla (Figure 2). This transition from mobile sands to hardgrounds is associated with the Rose Canyon Fault, which lines up with La Jolla Canyon, and delineates the northern extent of Mount Soledad. In turn, the Country Club Fault correlates with a zone of increased seafloor roughness that occurs immediately south of La Jolla Canyon. The Country Club Fault is also associated with differences in erosion patterns along the sea cliffs. South of the Country Club Fault and north of the Mount Soledad Fault, rocks are sand-dominated whereas in between these two faults the rocks are mud-dominated.

3.3 Sedimentary Units Offshore La Jolla

3.3.1 Sequence I: Canyon-Edge Deposits

The lowest unit interpreted in the seismic profiles is characterized by parallel, highly reflective horizons inter-bedded with acoustically transparent sediments. Sequence I onlaps existing topography, is locally truncated by the overlying transgressive surface, and is deposited above the inferred sequence boundary (Figures 6A, 7A, and 8). These layers tend to attenuate the acoustic source energy, which generally precludes imaging of deeper stratigraphic units. Divers sampled Sequence I at ~23 m depth in the head of La Jolla Canyon and recovered push cores containing fine-grained muds interbedded with silts and sands (Figures 2, 3B, and 6C). An isopach map of these laminated sediments shows that they occur along the canyon edges (Figure 6D). These sediments have a large spatial extent at the head of La Jolla Canyon, whereas they are confined to the edges of Scripps Canyon. Furthermore, the sediments of this unit are thicker near La Jolla Canyon (> 10 m thick) than in Scripps Canyon.

3.3.2 Sequence II: Infilling Unit

Within the sediments overlying the transgressive surface, a basal unit exhibiting distinct lamination is observed (Figure 7). The acoustic character of these sediments is different from the unit observed near the canyons; as they are sub-parallel, highly reflective horizons inter-bedded with unevenly reflective layers. The unit is spatially limited to the lows in the transgressive surface between the two canyons and to the north of Scripps Canyon (Figures 5, 7, and 8). These laminated sediments are thickest, up to 12 m thick, seaward of the 30 m isobath. Moreover, these deposits infill lows and diminish relief on the transgressive surface (Figures 5 and 7B). In dip lines, between ~70 m and 35 m water depth, the onlapping reflectors within Sequence II have high acoustic amplitudes at their landward terminations, but the amplitudes diminish seaward, where they eventually become acoustically transparent. Some of the layers exhibit downlap onto older deposits within this sequence or onto the underlying transgressive surface.

The isopach map in Figure 10B details the thickness and distribution of Sequence II deposits. The thickest accumulation fills a structural low on the transgressive surface just to the north of Scripps Canyon (Figures 8 and 9B). Sequence II is absent landward of the 20-m bathymetry contour (Figures 8 and 10B). Although the thickness of the entire sedimentary sequence above the transgressive surface is variable (Figure 10A), most of the observed lateral variability is associated with Sequence II (Figure 10B).

3.3.3 Sequence III: Upper Unit

The uppermost unit is acoustically transparent, exhibits cross-shelf thickness variability with a mid-shelf depocenter, and makes up the majority of sediment overlying the transgressive surface (Figures 7 and 8). The unit is fine-grained to very fine-grained, homogenous sands based on cores acquired in the area (Figure 2; Darigo and Osbourne, 1986; Hogarth et al., 2007). In areas where these acoustically transparent sediments overlie the transgressive surface, there is a clear transition, but the transition between Sequences II and III can be less distinct. The laminations of Sequence II grade upward into the transparent Sequence III and in some areas fade into the transparent unit approaching their lateral terminations (Figure 7). Thus, the boundary between the basal unit and the overlying sediments was selected at the uppermost identifiable reflector.

Despite being acoustically transparent, the unit does contain several subtle, oblique or occasionally curved reflectors. In strike lines at the canyon edges, as the seabed slope increases, these reflectors dip towards the canyon axis and, where curved, are generally concave upwards. In general, the reflectors originate at or near the seabed, and sometimes occur in sets of two or three reflectors. The geometry of these features is similar to the shape of the seafloor observed along the modern canyon edges. Where the reflectors intercept the basal highly-reflective package (Sequence II) near the canyon edges, they appear to truncate the underlying reflectors and also exhibit a change in trend from concave up to concave down. Several profiles exhibit an apparent increase in thickness of the transparent sediment unit in close proximity to the canyon due to the oblique orientation of side channels (Figures 3B and 7A). This creates a concave-up geometry of the seabed in strike profiles crossing the canyon, reflecting the three-dimensionality of these side channels.

An isopach map showing the combined thickness of Sequences II and III (Figure 10A), illustrates how these sequences infill topographic relief along the transgressive surface (Figure 9B). In the isopach map (Figure 10A), from south to north, we observe the following: 1) Holocene sediment is absent on top of the hard grounds south of La Jolla Canyon, 2) a depocenter containing > 20 m of sediment overlies the erosional surface between the two branches of the canyon, 3) a second depocenter north of Scripps Canyon also contains > 20 m of sediment, and 4) sediment thickness thins to ~5 m across the zone that extends between Scripps Canyon and the northern extent of the study area, which corresponds to the pop-up structure identified by Hogarth et al. (2007).

As previously mentioned, much of the variability in the thickness of the Holocene unit (Figure 10A) corresponds to variability in the basal, reflective package (Figure 10B). This basal unit makes up most of the depocenter north of Scripps Canyon (Figure 10B), whereas the upper transparent unit accounts for the majority of sediment in the depocenter between the two canyons (Figure 10C). In addition, to the north of Scripps Canyon, the overlying acoustically transparent unit (Figure 10C) reveals a well-developed mid-shelf depocenter along the 40 m depth contour. Note the slight seaward deflection of the mid-shelf depocenter toward the north offshore Torrey Pines State Park, reflecting deformation on the constraining bend and uplifted pop-up structure (Hogarth et al., 2007).

4. Discussion

4.1 Tectonic control on canyon location

Although researchers have long proposed that the RCFZ controls the location of La Jolla Canyon (e.g., Shepard, 1981; Trieman, 1993), the seismic and swath data provide new constraints on regional tectonic deformation and the distribution of post-Last Glacial Maximum (LGM, ~21 ka) sedimentary sequences. Bedding planes beneath the transgressive surface exhibit widespread dip reversals to the north of La Jolla Canyon (Figure 4). The relatively steep dip of these units near La Jolla Canyon appears to be the result of compression along the constraining bend north of Mt. Soledad (Figure 4). Farther east onshore, bedding mapped by Kennedy (1975) dips more shallowly because the fault is more translational in this region. Similar dip reversals have been observed in other regions where folding and faulting have been documented (e.g., Gulick and Meltzer, 2002).

The seismic and bathymetric data suggest that Scripps Canyon formed at the apex of a structural antiform (Figure 4). While other rectilinear canyons extending close to the coastline appear to be fault controlled (e.g., the Redondo Canyon; Gardner et al., 2002), none of the en-echelon oblique faults observed in adjacent sea cliffs project offshore to the location of Scripps Canyon (Figure 2). Shoaling of the transgressive surface associated with the antiform that appears to control Scripps Canyon is best expressed on the northern limb (Figures 4 and 9B). Anticlinal folding causes extension above the neutral surface and consequent fracturing parallel to the axis of the fold. In contrast, synclines as observed between the canyons and to the north of Scripps Canyon engender compression above the neutral surface that would minimize fracturing. We propose that erosion at the apex of this antiform would be enhanced due to the fractured and structurally weakened nature of the rock (Davis and Reynolds, 1996). Enhanced erosion along this shore-normal zone of fractures may have initiated formation of Scripps Canyon. The linear morphology of Scripps Canyon has led previous researchers to invoke a tectonic origin. Specifically, fractures related to the Torrey Pines Fault have been purported to exert a structural control on the orientation of the shallow water branches at the head of the canyon (Rindell, 1991; Webb, 1988). However, there is no evidence in seismic profiles of faults intersecting the heads of Scripps Canyon. In our scenario, these fractures are not fault-controlled, but are rather associated with folding and consequent extension across the crest of an antiform.

La Jolla Canyon is also located in an area with pronounced dip reversal, which is the result of the RCFZ (Figure 4). Onshore observations of the three main faults and of their offshore extensions imaged in the seismic data refine our understanding of the structural control on the formation of La Jolla Canyon (Figure 4). The thalweg of La Jolla Canyon occurs along a thrust fault in the RCFZ that separates lithified Cretaceous mudstones from less consolidated Eocene sands and gravels. The Country Club Fault, despite having large horizontal offset on land, has little influence on the location of the La Jolla submarine canyon because the Cretaceous rocks on both sides of the fault are well indurated. It appears that the canyon exploits the northernmost fault, which is the boundary between the competent Cretaceous formations and the less lithified Eocene sands and gravels.

4.2 Tectonic Control on Canyon Morphology

Tectonically induced structure governs the characteristics of the side channels that intersect La Jolla Canyon. The marked asymmetry exhibited by these side channels, being much larger on the northern wall, is likely controlled by lithologic differences across the Rose Canyon Fault (Figure 3). Short, arcuate cuts in the south wall of La Jolla Canyon occur where highly resistive Cretaceous lithified units are exposed. Side canyons on the northern wall of La Jolla Canyon incised more deeply into the adjacent shelf due to the less indurated Eocene substrate. One of the larger incisions on the northern side of La Jolla Canyon appears to be controlled by the northeast-southwest trending Scripps Fault (Figure 2 and “S” in Figure 3). This side canyon trends to the northeast for ~500 m, but abruptly curves to the north at its head.

In contrast to La Jolla Canyon, the side canyons along Scripps Canyon incise only the upper surficial sediments that are unlithified, and as a result are much less steep (Figure 2). Observations of recurring sediment accumulation and subsequent catastrophic slump events indicate that some of the secondary canyon tributaries are active (Dill, 1964; Marshall, 1978). The oblique intersection of these secondary incisions with the thalweg of Scripps Canyon suggests formation by downslope-eroding sediment flows, rather than by retrogressive failure alone, which would yield a more orthogonal geometry (Farre et al., 1983). In addition, Mastbergen and van den Berg (2003) recently proposed a breaching model based on negative pore pressure build-up and tested it on a well-documented slide in the south wall of Scripps Canyon (Marshall, 1978). The role of slope failure in forming these channels is apparent in the shape of the canyon edges. The steep upper walls appear to be formed by failure of unconsolidated Holocene deposits. In addition, there is no observed down-lap in the strike lines across Scripps Canyon that would be indicative of the non-deposition and sediment bypass associated with strong axial canyon currents (Figure 7).

The influence of the canyon on the adjacent morphology as observed in the bathymetry is over a much greater distance than would be predicted by slope stability (Figures 3 and 7A). The upper walls of Scripps Canyon and along the north side of La Jolla Canyon, the slopes should not exceed the angle of repose for saturated sands as the sediments are unconsolidated. It is interesting to note, the slopes of the side canyons are significantly below the angle of repose yet they extend up to one kilometer away from the thalweg. These observations suggest other factors in addition to slope stability may shape the side canyons.

4.3 Tectonic control on sediment distribution and thickness

Three sedimentary units and their relative ages have been identified in the seismic data based on stratal geometry, acoustic character, and analyses of sediment samples where available. We interpret Sequence I, the highly reflective unit observed near the canyons and sampled by push cores, as an estuarine or lagoonal deposit, consistent with previous findings that the sediments within the head of La Jolla Canyon were deposited in an estuarine environment (Holden 1968; Judy 1987; Shepard and Dill, 1966). The presence of ostracods in sediment samples recovered from the head of La Jolla Canyon at water depths of 23 m (Holden, 1968) is indicative of deposition within a brackish water environment. Radiocarbon dates of root structures within the same horizon yielded ages of 8270±500 years b.p. (Holden, 1968; Shepard and Dill, 1966). Often age dates derived from woody debris overestimate the age of deposition as wood can have some residence time in the watershed, however, this does not apply to in situ root structures. The ostracods were found in sediments outcropping from 16 to 27 m water depth (Holden, 1968), which is consistent with the sediment thickness observed in CHIRP seismic data from this region. During transgression, the canyons may have acted as inlets to low lying areas landward of the beach similar to what is observed at Penasquitos Lagoon today. These low areas are potential locations where late-lowstand or early-transgressive subaerial deposits may be preserved between the sequence boundary and overlying transgressive surface. Similar estuarine units appear to be deposited along Scripps Canyon in similar water depths (Figure 6).

Farther offshore, we interpret Sequence II, the basal sediments infilling lows or notches in the transgressive surface (Figures 5 and 7), as a transgressive deposit, often referred to as a healing-phase wedge (Posamentier and Allen, 1999). Healing-phase deposits have been referred to as transgressive backfill or transgressive lag (e.g., Cattaneo and Steel, 2003 and references therein). Darigo and Osbourne (1986) interpreted this unit to be several different marine and nonmarine deposits of late Pleistocene age. Sequence III, the upper acoustically transparent unit is interpreted to be a late-transgressive to highstand unit comprising unconsolidated sands, consistent with Hogarth et al. (2007).

The geometries and locations of the three sedimentary units in the area reflect the interplay of tectonics, eustasy, and sediment supply. We are able to distinguish the influences of eustasy and local transpressional tectonics based on geometry; transpression on the RCFZ imparts a shore parallel trend while effects due to sea-level change and long-term, regional tectonic deformation engender a cross-shore trend (Hogarth et al., 2007). As sea level rises and a shoreline transgresses, areas of the coastal plain landward of the shoreline become potential areas of aggradation. In the case where sediment supply outpaces upper shoreface erosion, estuarine deposits can be preserved, in particular within channel incisions and embayments. As sea level continues to rise, erosion of the upper shoreface provides sediments to infill, or “heal,” the lows in the lower shoreface and on the shelf (Catuneanu, 2006; Posamentier and Allen, 1999). These lows usually occur seaward of notches that are likely a consequence of relative sea-level still stands (Figure 7B). In some cases, the location of these notches is also influenced by the presence of back-tilted blocks, which allowed for differential erosion (Figure 7B). The lows are subsequently backfilled as the shoreline migrates landward, eroding the coastline, with the consequent coarse-grained lag deposited offshore. As the transgression continues, so-called healing-phase deposits overlie the preserved estuarine sediments, as observed in strike lines (> 20 m) around Scripps Canyon (Figures 7A and 8).

As the Scripps and La Jolla submarine canyons cut across the entire shelf into the nearshore, the upper reaches of these features constitute embayments that are conducive to the deposition of estuarine sediments. In the case of La Jolla Canyon (Figure 6), estuarine deposits found at shallow depths (~10-15 m) are inferred to be late-Holocene in age as a lagoon still occupied this site only 100 years ago and extended ~1 mile to the east of the current La Jolla Shores Beach (Moriarty, 1964). These thick estuarine deposits crop out in some areas, in particular along isolated ridges within the head of La Jolla Canyon (Figure 6). Most likely, wave and tidal energy efficiently reworks sediments or prevents the deposition of modern sands over the estuarine units that outcrop at shallow water depths.

Beyond the primary features controlled by eustasy and long-term tectonic deformation, we observe tectonically induced secondary relief on the transgressive surface. The pop-up structure associated with the constraining bend on the Rose Canyon Fault generates a local northward shoaling trend on the transgressive surface (Figure 9). The antiform through which Scripps Canyon is incised is an influential secondary structure as well. Operating at smaller wavelengths, deformation and offset bedding associated with east-west trending faults create along shore variability in the transgressive surface and appear to influence the pattern of modern sediment deposition. The most significant example of this deformation is the localized structural high north of Scripps Canyon associated with the Carmel Valley and Salk faults on land (Figures 4 and

8). The area between these two oblique faults appears to be uplifted relative to the surrounding area (Figures 1 and 5). Both the large-wavelength uplift associated with the pop-up structure and the short-wavelength deformation associated with these oblique faults create along-shore relief in the transgressive surface (Figures 4, 5, and 9B).

The healing-phase wedge is confined to the saddle region away from the canyons. Similar infilling of lows in the antecedent topography during transgression has been observed elsewhere (e.g., on the northern California shelf, Sommerfield and Wheatcroft, 2007). North of Scripps Canyon, the northern Holocene depocenter and much of the along-shore thickness variability observed in the Holocene sequence corresponds to variations in the basal healing-phase unit (Figures 10A and 10B). Such a correlation is not observed in the inter-canyon shelf where the transparent upper sands appear to account for the majority of the sediment thickness in the depocenter (Figures 10A, 10B, and 10C). The depression in the transgressive surface is more pronounced north of Scripps Canyon than in the inter-canyon shelf (Figure 9B). This is likely due to the positive uplift associated with the pop-up structure to the north and the shoaling of the transgressive surface towards the RCFZ in the south. The reflectors observed in the healing-phase deposits of the main depocenter are horizontal and on-lap the transgressive surface (Figure 7A). This indicates that offset on the Carmel Valley and Salk faults, and more importantly, uplift of the pop-up structure pre-date deposition of the healing-phase unit.

Some of the relief on the transgressive surface is modified by wave erosion in the nearshore, which enhances the smoothness of the seafloor as coarse-grained sediments eroded from the shoreface are transported to the low areas offshore (Figure 10B). For example, fault-induced roughness in the transgressive surface is preserved in deeper water because these areas were more rapidly transgressed. We interpret the overall decrease in the relief on the transgressive surface from offshore to onshore, which greatly influences the location of healing-phase deposits, as a consequence of the varying rates of sea-level rise during the last transgression (Figure 5; Fairbanks, 1989). With decreasing rate of sea-level rise, the shallower part of the shelf was exposed to wave-based erosion over a longer period and existing structures were more effectively leveled. This pattern of increased roughness offshore is likely enhanced by the overprinting of erosion during several sea-level cycles.

4.4 Hydrodynamic control on modern sediment accumulation

The distribution of the upper Holocene sediment package in the along-shore direction is affected by hydrodynamic factors (wind, waves, and currents), sediment supply, and antecedent topography. Based on the acoustic character change between Sequences II and III and limited core data, we infer the change in acoustic character records a change in sediment sorting from coarse-grained, poorly sorted sediment to fine-grained, well sorted sands. Given the 8270 y.b.p. age for underlying estuarine sediments (Holden, 1968; Shepard and Dill, 1966), this sets the upper age limit for the overlying acoustically transparent sequence. The structure contour map of the top of Sequence II (Figure 9C) shows that the relief along the transgressive surface (Figure 9B) has been diminished by the healing-phase wedge, leaving a relatively smooth inner shelf profile with a seaward dip and minor along-shore variability. North of Scripps Canyon, unconsolidated sediments are thickest at ~40 m water depth (Figure 10C) and thin both seaward and landward (Figures 7B, 8, 10A, and 10C). The depocenter records the depth to which average waves can transport sediment seaward (Figure 10C). Offshore transport beyond the depocenter only occurs infrequently during larger events, which may explain the observed offshore thinning (e.g., Harris and Wiberg, 2001; Henry, 1976; Zhang et al., 1999).

In the northern part of our survey area, offshore Torrey Pines State Park, very little modern sediment deposition occurs at shallow water depths as the mid-shelf thickness high is deflected seaward due the shoaling of the transgressive surface (Figures 10A and 10C). The marked thinning of Sequence II in the deeper area of our survey corresponds to the deformation associated with oblique faults as little sediment has accumulated over the transgressive surface high (Figure 5). Because the healing-phase infilled and reduced relief across the transgressive surface offshore, minimal thickness variation in the overlying transparent package is observed in this region (Figures 9C and 10C).

Our work questions the efficiency of Scripps Canyon in capturing and transporting sediment offshore during the most recent sea-level rise and challenges the prevailing views of Holocene sediment transport and deposition offshore La Jolla. Observation of sediment wasting events in the heads of Scripps Canyon (Chamberlain, 1964; Dill, 1964) and related studies involving mass balance estimates for littoral cell sediment budgets (Inman and Chamberlain, 1960; Inman and Masters, 1991b) have led the research community to conclude that the majority of sediment is captured and transported offshore by Scripps Canyon. However, our data shows that modern sediment accumulation offshore La Jolla may be more complex. The well-defined thickness maximum in the upper acoustically transparent layer, which corresponds to the inter-canyon Holocene depocenter, requires a net influx of sediment to this region since ~6-8 ka.

Mass balance calculations by Chamberlain (1964) suggested that much of the sediment supplied by longshore drift escaped the littoral cell via Scripps Canyon. Nevertheless, our observations suggest that large amounts of sediment have bypassed Scripps Canyon, despite the narrow pathway between the canyon head and the beach. The large along-shore variation in wave heights observed near Scripps Canyon may be a mechanism for enhanced sediment transport within the surf zone shoreward of the Scripps Canyon head. Thus, we need to reassess the role of the La Jolla Canyon System on sediment accumulation on the inner shelf and evaluate the proportion of sand captured by the canyon versus that shunted southward to the inter-canyon depocenter.

Observations of modern sediment accumulation on the San Diego County shelf, which provide a perspective on the regional pattern, confirm that the inner shelf offshore La Jolla, California is generally a depocenter of modern sediments. Regional studies reveal that exposed bedrock is common between the mid-shelf wedge and the beach, except at river mouths (Henry, 1976). Outside of the two areas of uplift due to the RCFZ, there are no bedrock exposures offshore La Jolla between the mid-shelf wedge and the beach. Our study area appears to be characterized by an atypically large accumulation of young sediment. The westward step of the coastline at the southern extremity of the Oceanside littoral cell may act as a jetty and promote sediment accumulation. The well-developed rip currents consistently observed south of the Scripps Pier at La Jolla Shores beach (Shepard and Inman, 1950) and also immediately north of the Scripps Pier (Smith and Largier, 1995) are likely contributing to this net accumulation. These currents redistribute modern sediments seaward on the inter-canyon shelf (Inman, 1952; Inman, 1953) to form the depocenter observed in the isopach maps.

Repeated sounding surveys performed between 1949 and 1950 (Inman, 1952; Inman, 1953; Shepard and Inman, 1951) and seismic surveys conducted in 1976 and 1979 with a 3.5 kHz seismic profiler (Henry, 1976; Waggoner, 1979) indicate that sand levels are fairly stable on short time scales (1 to 3 years) at the location where we have identified the upper Holocene depocenter in the inter-canyon shelf. However, both accretion and erosion dynamics have been reported (Dayton et al., 1989; Inman, 1953; Marshall, 1978). This would imply that the Holocene sediment depocenter is currently in near equilibrium, with little net influx or outflux over at least the last few decades. A well-defined scour mark due to dredging is observed at 20 m water depth to the north of our study area (see Dartnell, et al., 2007). The preservation of this feature after the dredging occurred indicates that longshore drift is currently limited to the nearshore region. Sediment transport in the littoral cell may be highly episodic with sediment transport occurring during abnormally stormy climatic regimes.

5. Conclusions

High-resolution three-dimensional coverage of the shelf in the vicinity of the La Jolla and Scripps submarine canyons, obtained from CHIRP seismic and swath bathymetry data, highlights the structural control on the observed stratigraphy and morphology. The faulted and folded tectonic landscape associated with constraining bends in the Rose Canyon Fault Zone plays a critical role in canyon location and morphology as well as in the distribution of modern facies offshore La Jolla, California. In addition to the northward shoaling of the transgressive surface, our high-resolution seismics reveal much cross-shore and along-shore structural variability. We observe widespread dip reversals in the bedrock and an increased dip of offshore units compared to those observed onshore. We propose that the observed structural deformation offshore La Jolla is the expression of the compressional component of the transpressional strain regime associated with the RCFZ. We also propose that an antiform controls the location of Scripps Canyon, contrary to the previous hypothesis of fault control. Furthermore, the action of wave-based erosion is reflected in leveling and smoothing of bedrock highs and subsequent infilling of lows with reworked shelf materials. There is also an overall decrease of relief and small-scale roughness in the transgressive surface landward of ~25 m water depth due to a decrease in the rate of sea-level rise and longer exposure to wave-base erosion.

The detailed bathymetry reveals morphological differences between La Jolla Canyon and Scripps Canyon at various scales, from overall canyon shape to morphology of secondary incisions. The asymmetric development and deep side channels of La Jolla Canyon are indicative of differential erosion due to deformation near the RCFZ. The longitudinal variability of the unconsolidated modern sediment cover on the upper walls of Scripps Canyon appears to result from erosion of shallow gullies by failure processes. Ancient failures or sliding planes within the upper Holocene unit record the evolutionary history of the canyon edges.

We identify three stratigraphic sequences overlying acoustic bedrock offshore La Jolla: 1) estuarine deposits, 2) a healing-phase wedge, and 3) homogeneous sands. We interpret the spatial distribution of these modern stratigraphic units in light of the complex interaction between sea-level rise, tectonics, and sediment supply. The primarily along-shore variation in the local tectonic structure allows us to distinguish the influences of eustasy and transpressional tectonics. The deposition pattern of the two older packages appears to be structurally controlled, with lagoonal deposits limited to the shallow upper reaches of the canyons and the healing-phase deposits infilling the lows seaward of wave-cut notches. The accumulation of the younger sand unit is controlled in large part by local hydrodynamics, with a typical mid-shelf depocenter north of Scripps Canyon and between the canyons. The identification of this depocenter raises questions about the efficiency of Scripps Canyon in capturing sediments and refines our conceptual model for the Holocene sediment transport and deposition offshore La Jolla.

Acknowledgements

This research was funded by the Office of Naval Research, the Southern California Coastal Ocean Observing System (SCCOOS), and an Achievement Rewards for College Scientists (ARCS) fellowship. We thank William W. Danforth for his help processing the Submetrix data, Warren L. Smith for his assistance in analyzing cores, Captain Eddy Kisfaludy for operating the R/V Saihkon, the crew of the R/V Sproul, and Douglas Inman for numerous discussions on the topics in this manuscript. We would also like to thank Wayne Baldwin, Daniel Belknap, and an anonymous reviewer for their comments, which improved the manuscript. The authors also acknowledge the use of software packages for data processing. The Generic Mapping Tools (GMT, Smith and Wessel, 1990; Wessel and Smith, 1998; http://gmt.soest.hawaii.edu) and Mirone (Luis, 2007; http://w3.ualg.pt/~jluis/mirone) are available online free of charge. Kindgom Suite (http://www.seismicmicro.com) is commercial software made available for educational use at no charge.

References

Belknap, D.F., Kraft, J.C., 1985. Influence of antecedent geology on stratigraphic preservation potential and evolution of Delaware's barrier systems. Marine Geology, 63, 235-262.

Buckingham, M.J., Richardson, M.D., 2002. On tone-burst measurements of sound speed and attenuation in sandy marine sediments. IEEE Journal of Oceanic Engineering, 27 (3), 429-453.

Buffington, E.C., 1964. Structural control and precision bathymetry of La Jolla submarine canyon, California. Marine Geology, 11, 44-58.

Byrd, R.E., Berry, R.W., Fischer, P.J., 1975. Quaternary geology of the San Diego - La Jolla underwater park. IN: Studies of the geology of Camp Pendelton and Western San Diego County, CA. San Diego Association of Geologists, 77-79.

Catuneanu, O., 2006. Principles of Sequence Stratigraphy. Amsterdam, Elsevier, 375 p.

Cattaneo, A., Steel, R.J., 2003. Transgressive deposits: a review of their variability. Earth-Science Reviews, 62 (3-4), 187.

Chamberlain, T.K., 1964. Mass transport of sediment in the heads of Scripps submarine canyon, California. IN: Papers in Marine Geology, Shepard Commemorative Volume. R.L. Miller, New York, Macmillan Company, 42-64.

Christie-Blick, N., Driscoll, N.W., 1995. Sequence stratigraphy. Annual Review of Earth and Planetary Sciences, 23, 451-478.

Cohen, J.K., Stockwell, Jr. J.W., 2002. CWP/SU: Seismic Unix release 36, a free package for seismic research and processing. Center for Wave Phenomena, Colorado School of Mines, Golden, Colorado, www.cwp.mines.edu/cwpcodes.

Covault, J.A., Normark, W.R., Romans, B.W., Graham, S.A., 2007. Highstand fans in the California borderland: the overlooked deep-water depositional systems. Geology, 35, 783-786.

Darigo, N.J., Osbourne, R.H., 1986. Quaternary stratigraphy and sedimentation of the inner continental shelf, San Diego County, California. IN: Knight, R.J., McLean, J.R., eds., Shelf sands and sandstones. Canadian Society of Petroleum Geologists Memoir II, 73-98.

Dartnell, P., Normark, W.R., Driscoll, N.W., Babcock, Gardner, J.M., Kvitek, J.V., Rikk, G., Iampietro, P.J., 2007. Multibeam bathymetry and selected perspective views offshore

San Diego, California. U.S. Geological Survey Scientific Investigations Map 2959, 2 sheets, version 1.0, June 14, 2007, http://pubs.usgs.gov/sim/2007/2959/.

Davis, G.H., Reynolds, S.J. 1996. Structural Geology of Rocks and Regions. New York, Wiley and Sons, 776 p.

Dayton, P.K., Seymour, R.J., Parnell, P.E., Tegner, M.J., 1989. Unusual marine erosion in San Diego County from a single storm. Estuarine, Coastal and Shelf Science, 29 (2), 151-160.

Dill, R.F., 1964. Sedimentation and erosion in Scripps submarine canyon head. IN: Papers in Marine Geology, Shepard Commemorative Volume. R.L. Miller, New York, Macmillan Company, 23-41.

Emery, K.O., 1958. Shallow submerged marine terraces of Southern California. Geological Society of America Bulletin, 69 (1), 39-60.

Everts, C.H., Dill, R.F., 1988. Sedimentation in submarine canyons, San Diego County, California, 1984-1987. US Army Corps of Engineers, Coastal Engineering Research Center, Waterways Experiment Station, Reference No. CSTWS 88-2.

Fairbanks, R.G., 1989. A 17,000-year glacio-eustatic sea-level record: influence of glacial melting rates on the Younger Dryas event and deep-ocean circulation. Nature, 342, 637-642.

Farre, J.A., McGregor, B.A., Ryan, W.B.F., Robb, J.M., 1983. Breaching the shelf break: passage from youthful to mature phase in canyon evolution. IN: The shelfbreak: critical interface on continental margins. Society of Economic Paleontologists and Mineralogists (SEPM) Special Publication No. 33, edited by Stanley, D.J., and Moore, G.T., Tulsa, Oklahoma, 25-40.

Gardner, J.B., Dartnell, P., Stone, C.J., Mayer, L.A., Hughes Clarke, J.E., 2002. Bathymetry and selected perspective views offshore greater Los Angeles, California. USGS - Water Resource Investigations Report 02-4126, 1 map sheet, http://walrus.wr.usgs.gov/pacmaps/pubs.html.

Gulick, S.P.S., Meltzer, A.S., 2002. Effect of the northward-migrating Mendocino triple junction on the Eel River forearc basin, California: structural evolution. Geological Society of America Bulletin, 114 (12), 1505-1519.

Harris, C.K., Wiberg, P.L., 2001. A two-dimensional, time-dependent model of suspended sediment transport and bed reworking for continental shelves. Computers & Geosciences, 27 (6), 675-690.

Harris, M.S., Gayes, P.T., Kindinger, J.L., Flocks, J.G., Krantz, D.E., Donovan, P., 2005. Quaternary geomorphology and modern coastal development in response to an inherent geologic framework: an example from Charleston, South Carolina. Journal of Coastal Research, 21 (1), 49–64.

Hass, J.K., 2005. Grain size and mineralogical characteristics of beach sand in the Oceanside Littoral Cell, Southern California: implications for sediment provenance. Thesis (M. S.)-University of California, San Diego.

Henkart, P., 2003. SIOSEIS software. Scripps Institution of Oceanography, La Jolla, California, http://sioseis.ucsd.edu.

Henry, M.J., 1976. The unconsolidated sediment distribution on the San Diego County mainland shelf, California. Masters thesis, San Diego State University.

Hogarth, L.J., Babcock, J., Driscoll, N.W., Le Dantec, N., Hass, J.K., Inman, D.L., Masters, P.M., 2007. Long-term tectonic control on Holocene shelf sedimentation offshore La Jolla, California. Geology, 35 (3), 275-278.

Holden, J.C., 1968. Brackish water ostracods from La Jolla submarine canyon 7200 (plus/minus) 500 years before present. Paleobios, No. 5, University of California, Berkeley, Museum of Paleontology.

Honeycutt, M.C., Krantz, D.E., 2003. Influence of the geologic framework on spatial variability in long-term shoreline change, Cape Henlopen to Rehoboth Beach, Delaware. Journal of Coastal Research, Special Issue No. 38, 147-167.

Inman, D.L., 1952. Areal and seasonal variations in beach and nearshore sediments at La Jolla, California. Ph. D. Thesis, University of California, Los Angeles.

Inman, D.L., 1953. Areal and seasonal variations in beach and nearshore sediments at La Jolla, California. US Dept of the Army, Corps of Engineers, Office of the Chief of Engineers, Beach Erosion Board, Technical Memorandum No. 39.

Inman, D. L., Chamberlain, T. K., 1960. Littoral sand budget along the southern California coast. Volume of Abstracts, Report of the 21st International Geological Congress, Copenhagen, Denmark, 245-246.

Inman, D.L., Nordstrom, C.E., Flick, R.E., 1976. Currents in submarine canyons; an air-sea-land interaction. Annual Review of Fluid Mechanics, 8, 275-310.

Inman, D.L., Masters, P.M., 1991a. Coastal sediment transport concepts and mechanisms. IN: Coast of California Storm and Tidal Waves Study, State of the Coast Report, Los Angeles, U.S. Army Corps of Engineers.

Inman, D. L., Masters, P. M., 1991b. Budget of sediment and prediction of the future state of the coast. IN: State of the Coast Report, San Diego Region, Coast of California Storm and Tidal Waves Study, U. S. Army Corps of Engineers, 5, 43.

Jackson, D.R., Briggs, K.B., Williams, K.L., Richardson, M.D., 1996. Tests of models for high-frequency seafloor backscatter. IEEE Journal of Oceanic Engineering, 21 (4), 458 – 470.

Judy, T.C., 1987. Reconnaissance geology of the Holocene lagoonal deposits in the La Jolla submarine canyon and their relationship to the Rose Canyon Fault. Undergraduate Research Report, San Diego State University.

Kennedy, M.P., 1975. Western San Diego metropolitan area: Del Mar, La Jolla, and Point Loma, 7 1/2 minute quadrangles. Bulletin, California, Division of Mines and Geology, Volume 200, 9–39.

Legg, M.R., Kennedy, M.P., 1979. Faulting offshore San Diego and Northern Baja, California. IN: Abbott, P.L., Elliott, W.J., eds., Earthquakes and other perils, San Diego region, San Diego, California, United States. San Diego Association of Geologists, 29–46.

Lindvall, S.C., Rockwell, T.K., 1995. Holocene activity of the Rose Canyon Fault zone in San Diego, California. Journal of Geophysical Research, B, Solid Earth and Planets, 100, 24121–24132.

Luis, J.F., 2007. Mirone: a multi-purpose tool for exploring grid data. Computers & Geosciences, 33, 31-41.

Marshall, N.F., 1978. Large storm-induced sediment slump reopens an unknown Scripps submarine canyon tributary. IN: Sedimentation in submarine canyons, fans, and trenches. Stanley, D.J., Gilbert, K., Stroudsburg, Pa, Dowden, Hutchinson and Ross, 73-84.

Mastbergen, D.R., van den Berg, J.H., 2003. Breaching in fine sands and the generation of sustained turbidity currents in submarine canyons. Sedimentology, 50 (4), 625-637.

McNinch, J.E., 2004. Geologic control in the nearshore: shore-oblique sandbars and shoreline erosional hotspots, Mid-Atlantic Bight, USA. Marine Geology, 221, 121-141.

Moore, G.W., 1972. Offshore extent of the Rose Canyon Fault, San Diego, California. U.S. Geological Survey Professional Paper P 0800-D, 113-116.

Moriarty, J.R., 1964. The use of oceanography in the solution of problems in a submarine archaeological site. IN: Papers in Marine Geology. R.L. Miller, New York, Macmillan, 511-522.

Peters, G., van Balen, R.T., 2007. Tectonic geomorphology of the northern Upper Rhine Graben, Germany. Global and Planetary Change, 58, 310-334.

Posamentier, H.W., Allen, G.P., 1999. Siliciclastic sequence stratigraphy: concepts and applications. SEPM, Concepts in Sedimentology and Paleontology, Volume 7, 210 p.

Pratson L.F., Haxby W.F., 1996. What is the slope of the U.S. continental slope? Geology, 24, 3-6.

Rindell, A.K., 1991. An investigation of Scripps submarine canyon: its geology, sedimentary regime, and bubbling gases. Masters Thesis, San Diego State University.

Schwab, W.C., Thieler, E.R., Allen, J.R., Foster, D.S., Swift, B.A., Denny, J.F., 2000. Influence of inner-continental shelf geologic framework on the evolution and behavior of the barrier-island system between Fire Island Inlet and Shinnecock Inlet, Long Island, New York. Journal of Coastal Research, 16 (2), 408-422.

Shepard, F.P., Emery, K.O., 1941. Submarine topography off the California coast: canyons and tectonic interpretation. Baltimore MD, Waverly Press.

Shepard, F.P., Inman, D.L., 1950. Nearshore water circulation related to bottom topography and wave refraction. Transactions of the American Geophysical Union, 31 (2), 196-212.

Shepard, F.P., Inman D.L., 1951. Sand movement on the shallow inter-canyon shelf at La Jolla, California. US Dept of the Army, Corps of Engineers, Office of the Chief of Engineers, Beach Erosion Board, Technical Memorandum No. 26.

Shepard, F.P., Dill, R.F., 1966. Submarine canyons and other sea valleys. Chicago, Rand McNally.

Shepard, F.P., McLoughlin, P.A., Marshall, N.F., Sullivan, G.G., 1977. Current-meter recordings of low-speed turbidity currents. Geology, 5 (5), 297-301.

Shepard, F.P. 1981. Submarine canyons: multiple causes and long-time persistence. American Association of Petroleum Geologists Bulletin 65 (6), 1062-1077.

Smith, J.A., Largier, J.L., 1995. Observations of nearshore circulation - rip currents. Journal of Geophysical Research - Oceans, 100 (6), 10967-10975.

Smith, W. H. F., P. Wessel, 1990. Gridding with continuous curvature splines in tension. Geophysics, 55 (3), 293-305.

Sommerfield, C.K., Lee, H.J., 2003. Magnitude and variability of Holocene sediment accumulation in Santa Monica Bay, California. Marine Environmental Research, 56, 151–176.

Sommerfield, C.K., Lee, H.J., 2004. Across-shelf sediment transport since the Last Glacial Maximum, southern California margin. Geology, 32 (4), 345–348.

Sommerfield C.K., Wheatcroft, R.A., 2007. Late Holocene sediment accumulation on the northern California shelf: oceanic, fluvial, and anthropogenic influences. Geological Society of America Bulletin, 119 (9-10), 1120–1134.

Stow, D.A., Chang, H.H., 1987. Coarse sediment delivery by coastal streams to the Oceanside Littoral Cell, California. Shore & Beach, 55 (1), 30-40.

Thieler, E.R., Pilkey, O.H.J., Cleary, W.J., Schwab, W.C., 2001. Modern sedimentation of the shoreface and inner continental shelf at Wrightsville beach, North Carolina, USA. Journal of Sedimentary Research, 71 (6), 958-970.

Thomson, J., Elgar, S., Herbers, T.H.C., 2005. Reflection and tunneling of ocean waves observed at a submarine canyon. Geophysical Research Letters, 32 (10), L10602.

Treiman, J.A., 1993. The Rose Canyon Fault Zone, southern California. California Division of Mines and Geology, Open File Report 93–02, 45 p.

Vetter, E.W., 1994. Hotspots of benthic production. Nature, 372, 47.

Waggoner, J.A., 1979. Unconsolidated shelf sediments in the area of Scripps and La Jolla submarine canyons. Masters of Science in Geology, San Diego State University.

Webb, D.A., 1988. A structural interpretation of Scripps submarine canyon. Advances in Underwater Science, Proceedings of the American Academy of Underwater Sciences, 8th Annual Scientific Diving Symposium, La Jolla, CA, American Academy of Underwater Sciences, 213-220.

Wessel, P., W. H. F. Smith, 1998. New, improved version of Generic Mapping Tools released. EOS Transactions of the American Geophysical Union, 79 (47), 579.

Williams K.L, Jackson D.R., Thorsos E.I., Tang D., Schock S.G., 2002. Comparison of sound speed and attenuation measured in a sandy sediment to predictions based on the Biot theory of porous media. IEEE Journal of Oceanic Engineering, 27 (3), 413.

Young, A.P., Ashford, S.A., 2006. Application of airborne LIDAR for seacliff volumetric change and beach-sediment budget contributions. Journal of Coastal Research, 22 (2), 307-318.

Zhang, Y., Swift, D., Fan, S., Niedoroda A., Reed, C., 1999. Two-dimensional numerical modeling of storm deposition on the northern California shelf. Marine Geology, 154 (1–4), 155-167.

Figure Captions

Figure 1. Regional map showing the left jog along the right-lateral Rose Canyon Fault and the consequent structural high on the inner shelf. Arrows indicate sense of strike-slip motion on the fault. Fault-induced scalloping is observed where the Rose Canyon Fault coincides with the shelf edge north and south of the pop-up structure. Bathymetry is modified from Dartnell et al. (2007) with a 20-m contour interval. Local faults shown in dotted black lines are based on Kennedy (1975) with D and U for downthrown and upthrown sides. CC=Country Club, MS=Mount Soledad, RC=Rose Canyon, Sc=Scripps, TP=Torrey Pines, Sa=Salk, and CV=Carmel Valley faults.

Figure 2. Ship tracks are shown (black lines) superimposed on high-resolution bathymetry. Core locations are denoted by purple stars (push core near La Jolla Canyon head and vibracore near the Scripps Pier south of Scripps Canyon). See Figure 1 for abbreviations.

Figure 3. High-resolution bathymetry near La Jolla Canyon System. A: View of high-resolution bathymetry near La Jolla and Scripps canyons. SC= Scripps Canyon, LJC= La Jolla Canyon, A=Canyon thalweg, W=Width of canyon thalweg, I=Incision into canyon wall (side channel), S=Sinuous side channel, C=Cretaceous hard grounds, R=Ridge within La Jolla Canyon head, D=Deflection of isobath shoreward, So=South Branch of Scripps Canyon, Su=Sumner Branch of Scripps Canyon, No=North Branch of Scripps Canyon. B: Perspective view looking east with core locations. Bathymetry has a vertical

exaggeration of 6:1, while the land has none.

Figure 4. Regional bedding dips. Black diamonds mark faults identified in seismic profiles. See Figure 1 for abbreviations. The outline of the canyon is superimposed in red. Cross-section from A to A' shows dipping reflectors beneath the transgressive surface (TS), inferred synforms and antiforms, and their relationship to Scripps and La Jolla canyons. Sequences II and III are shown.

Figure 5. Transgressive surface roughness increases with water depth. A: The offshore line, strike line 11, exhibits more roughness on the transgressive surface due to deformation on the Carmel Valley, Salk, and Torrey Pines faults. B: Strike line 10 is slightly shallower and exhibits significant smoothing of the transgressive surface. (M=multiple). Note Sequence II infills the lows. In location map, dotted line shows extent of bathymetry data and bold lines show profile locations.

Figure 6. A: Perspective image showing Sequence I outcropping at the seafloor. Bathymetry and seismic profile have vertical exaggeration of 6:1. Bold line on inset shows the profile location. B: Underwater photograph showing layers of Sequence I where push core was collected. C: Fine-grained sediment recovered in push core. D: Sequence I isopach map shows distribution and thickness of this unit and push core location. Red line outlines canyons and white lines are structure contours to the top of the transgressive surface.

Figure 7. CHIRP profiles. A: Strike line 8 uninterpreted (top) and interpreted (bottom) shows Sequences I, II, and III. Note that Scripps Canyon is located within a high in the transgressive surface. B: Dip line 3 uninterpreted (top) and interpreted (bottom) shows Sequences II and III. The terraces formed during relative sea-level still stands are more prominent at greater depths. (M=Multiple). Color code is as follows: red = Sequence I, green = Sequence II, and blue = Sequence III. Thick black line traces the transgressive surface. In location map, dotted line shows extent of bathymetry survey and bold lines show profile locations.

Figure 8. Seismic fence diagram revealing the regional distribution of Sequence I, II, and III. Sequence I (red unit) in this region is confined to the edges of Scripps Canyon. Dipping and truncated reflectors are observed beneath the transgressive surface and their dip varies along strike as shown in Figure 4. Sequence II (green unit) preferentially infills lows along the transgressive surface and thins landward. Northward thinning of Sequence III (blue unit) is observed in the study region. Profiles have a vertical exaggeration of 6:1. Inset shows figure location and seismic lines shown.

Figure 9. Structure contour maps. A: Bathymetry with 10 m contour interval in black. B: Depth to the transgressive surface with contours in black. C: Depth to the top of Sequence II with contours in black. For maps B and C, bathymetry contours are superimposed in white.

Figure 10. A: Isopach map of Sequences II and III. B: Isopach map of Sequence II. C: Isopach map of Sequence III. Note that Sequence II makes up most of the northern depocenter observed in A, whereas the inter-canyon depocenter is predominantly Sequence III. Isopach thicknesses are shown in black. For reference, the 40 m and 60 m structure contours to the top of the transgressive surface (white) and the outline of canyon (red) are superimposed. Note thickness scales vary for the different panels and were selected to highlight along-strike variability. Survey area is shown by dashed line, and gray regions within survey area are regions with zero sediment thickness.

Figure 1.

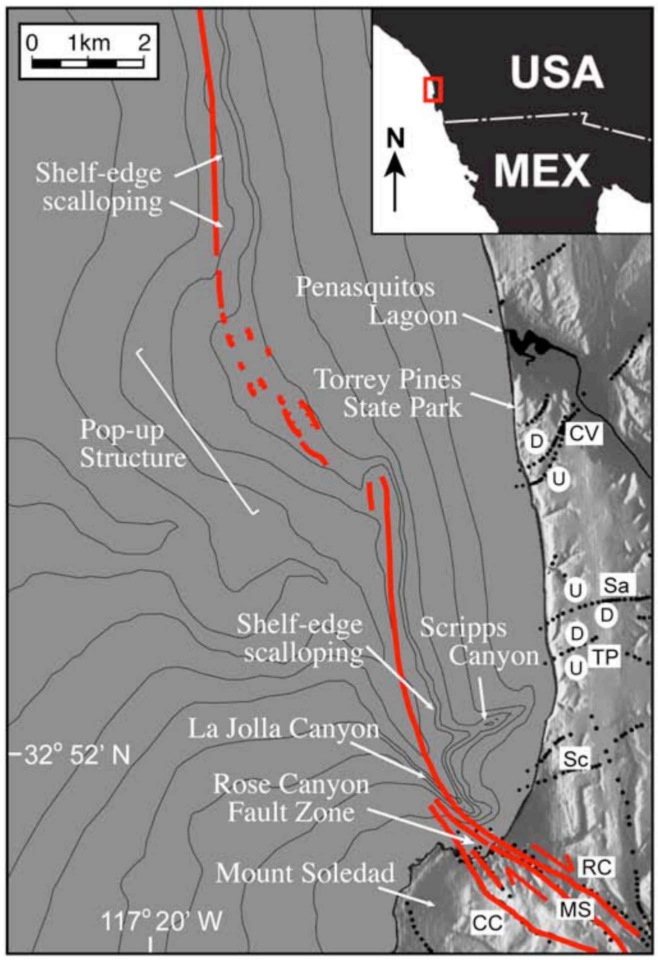
0 1km 2
USA
MEX
N
Shelf-edge scalloping
Penasquitos Lagoon
Torrey Pines State Park
Pop-up Structure
CV
D
U
Sa
TP
Shelf-edge scalloping
Scripps Canyon
La Jolla Canyon
32° 52' N
Sc
Rose Canyon Fault Zone
RC
Mount Soledad
MS
CC
117° 20' W

Figure 2.

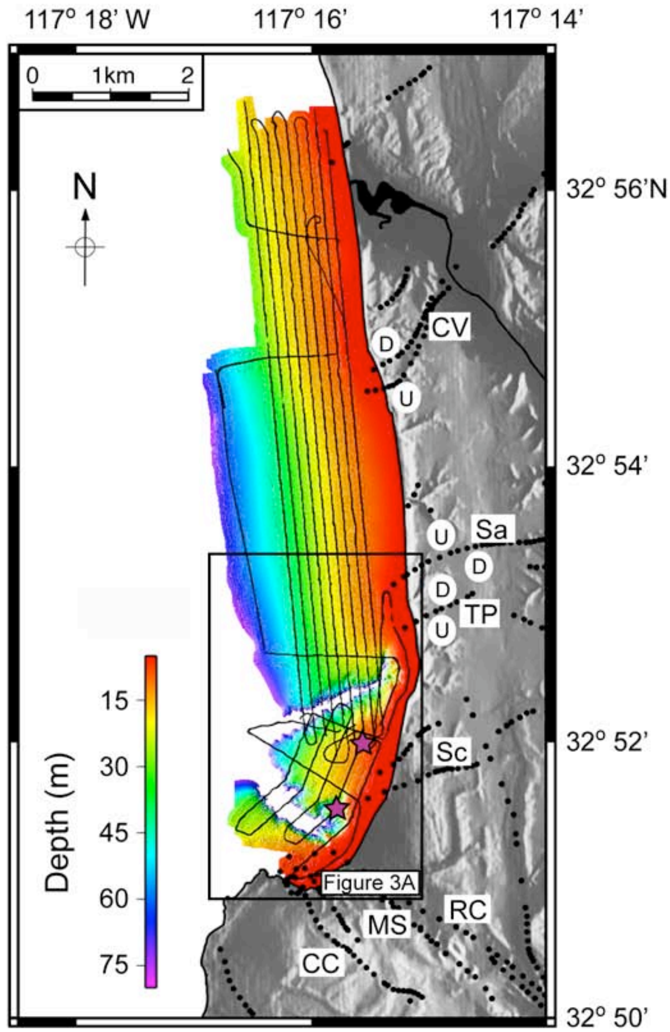

117° 18' W
117° 16'
117° 14'
32° 56'N
32° 54'
32° 52'
32° 50'
0
1km
2
N
CV
D
U
Sa
TP
Sc
RC
MS
CC
Figure 3A
Depth (m)
15
30
45
60
75

Figure 3.

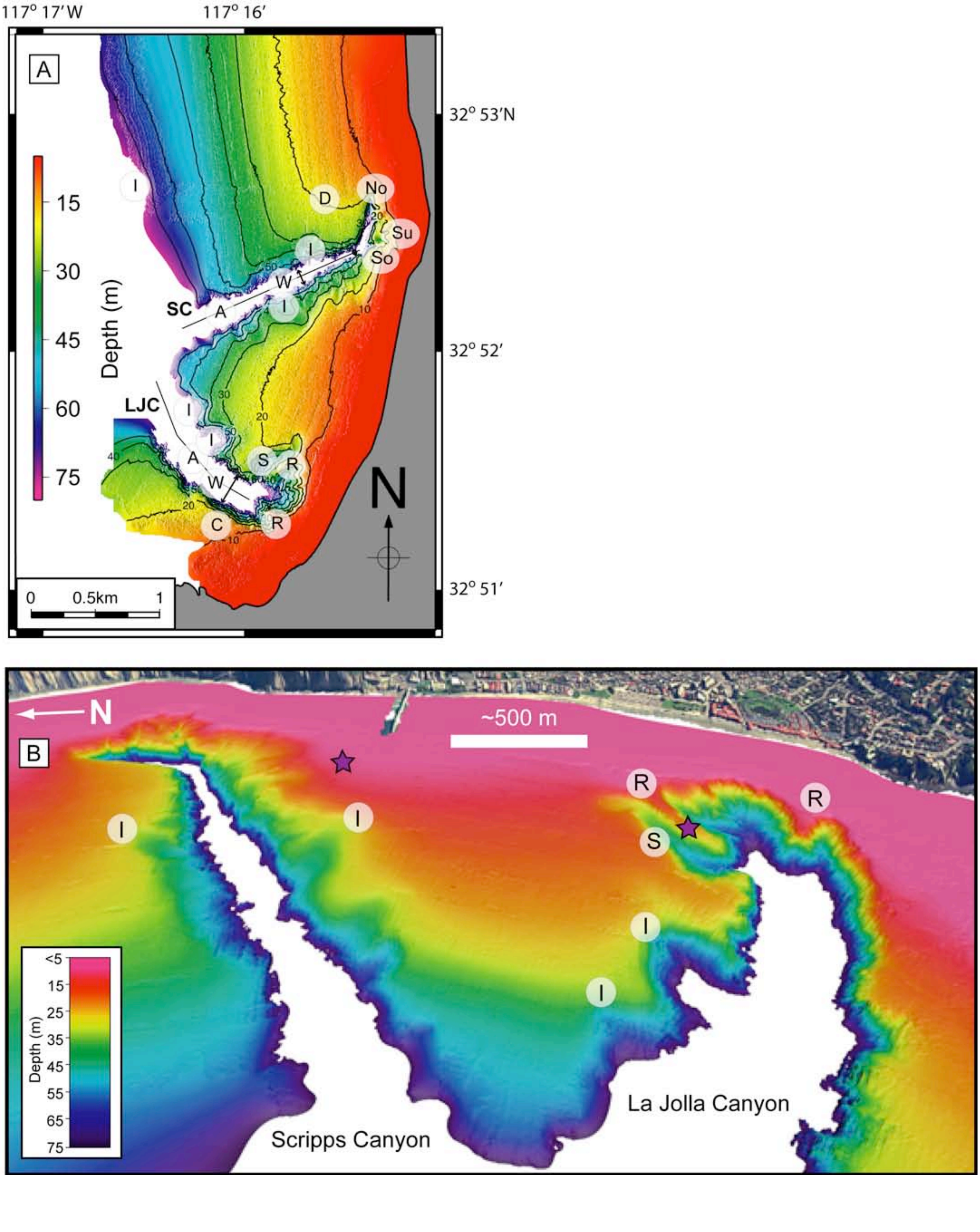
117° 17′ W
117° 16′
32° 53′N
32° 52′
32° 51′
A
Depth (m)
15
30
45
60
75
SC
LJC
No
Su
So
D
0
0.5km
1
N
B
N
~500 m
<5
25
35
55
65
Scripps Canyon
La Jolla Canyon

Figure 4.

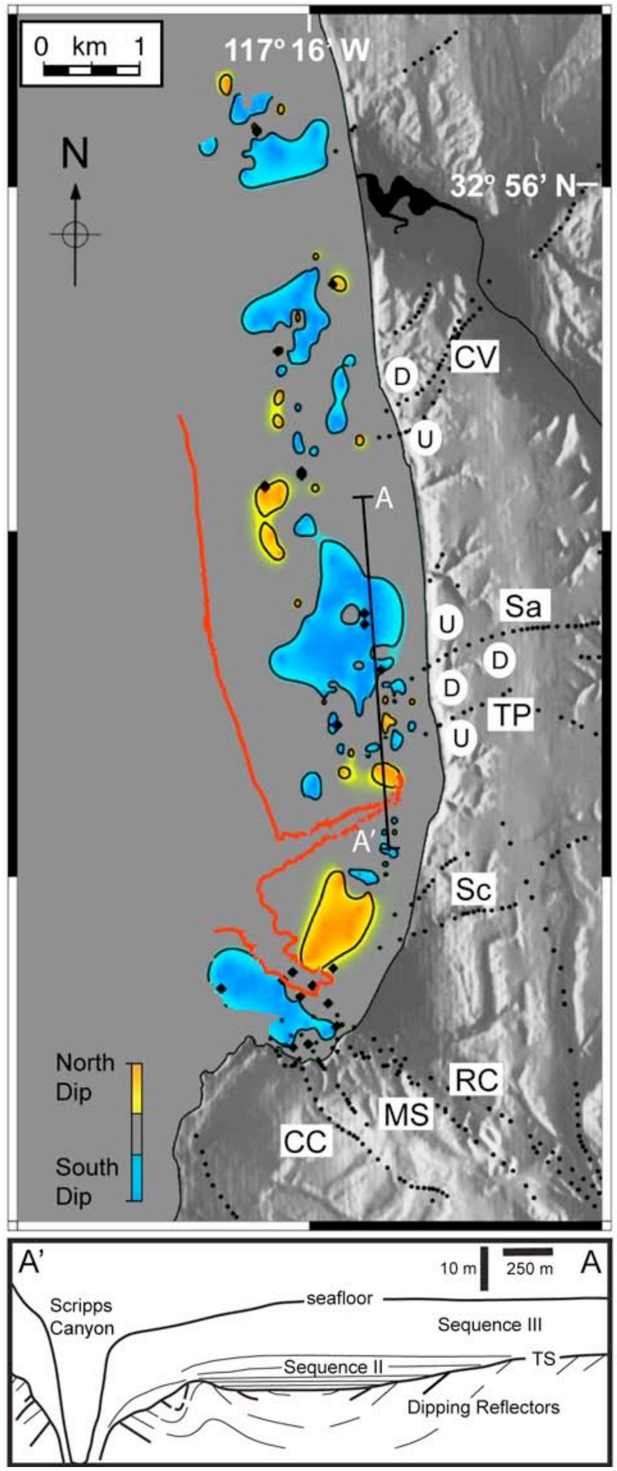

0 km 1
117° 16' W
N
32° 56' N
CV
D
U
A
Sa
U
D
D
TP
U
A'
Sc
RC
MS
CC
North Dip
South Dip
A'
10 m
250 m
A
Scripps Canyon
seafloor
Sequence III
Sequence II
TS
Dipping Reflectors

Figure 5.

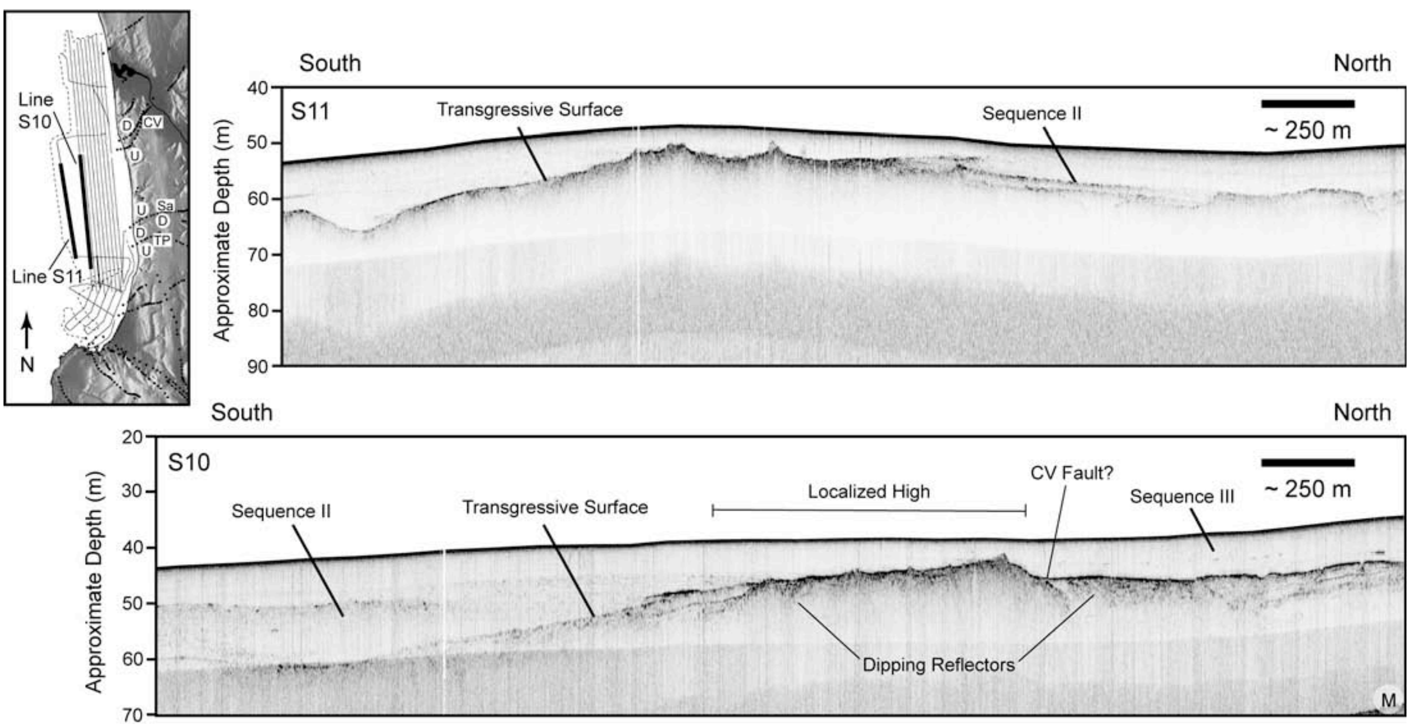

Line S10
Line S11
D
CV
U
U
Sa
D
D
TP
U
N
South
North
Approximate Depth (m)
S11
Transgressive Surface
Sequence II
~ 250 m
40
50
60
70
80
90
South
North
S10
Sequence II
Transgressive Surface
Localized High
CV Fault?
Sequence III
~ 250 m
Dipping Reflectors
Approximate Depth (m)
20
30
40
50
60
70
M

Figure 6.

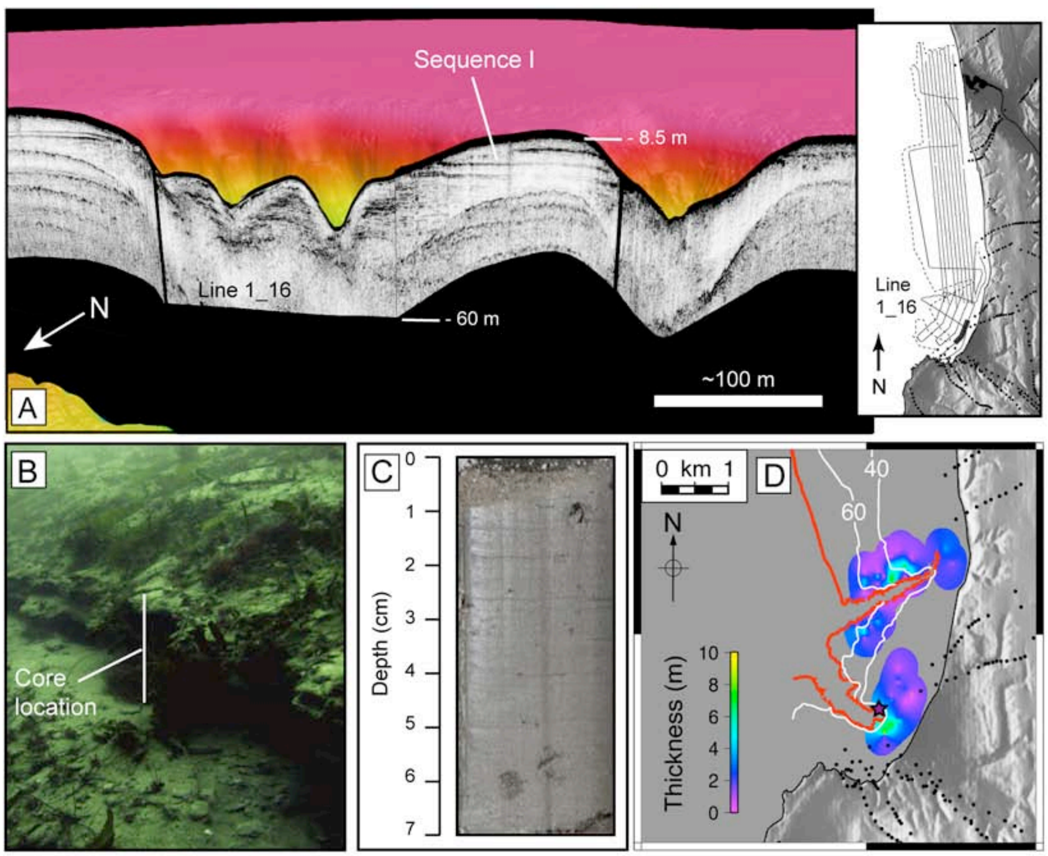
Sequence I
- 8.5 m
Line 1_16
N
- 60 m
~100 m
A
Line
1_16
N
B
Core
location
C
Depth (cm)
0
1
2
3
4
5
6
7
D
0 km 1
40
60
N
Thickness (m)
10
8
6
4
2
0

Figure 7.

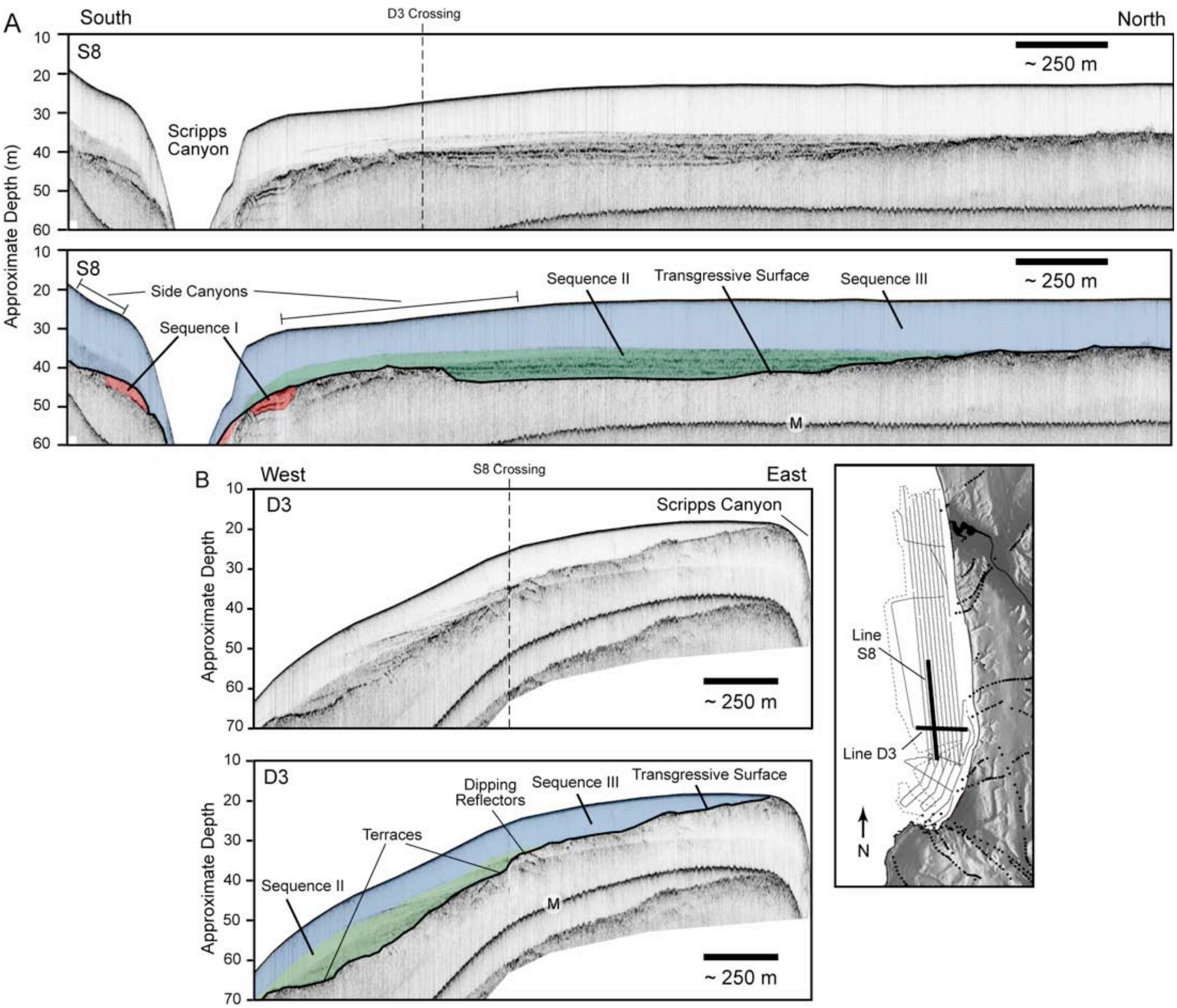

A
South
D3 Crossing
North
S8
~ 250 m
Scripps Canyon
Approximate Depth (m)
10
20
30
40
50
60
S8
Side Canyons
Sequence I
Sequence II
Transgressive Surface
Sequence III
~ 250 m
M
B
West
S8 Crossing
East
D3
Scripps Canyon
Approximate Depth
~ 250 m
70
D3
Dipping Reflectors
Sequence III
Transgressive Surface
Terraces
Sequence II
M
~ 250 m
Line S8
Line D3
N

Figure 8.

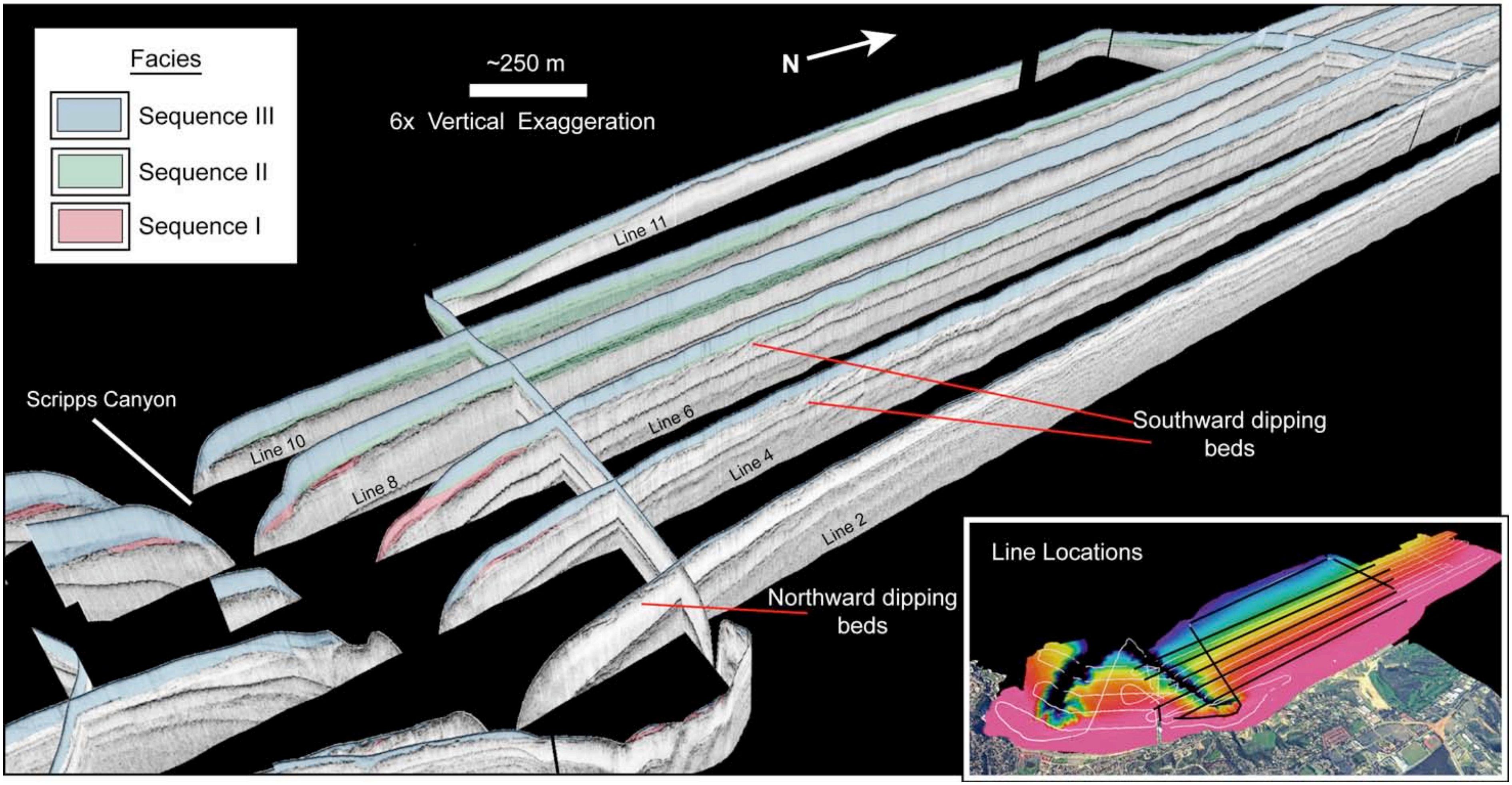

Facies
Sequence III
Sequence II
Sequence I
~250 m
6x Vertical Exaggeration
N
Line 11
Line 10
Line 8
Line 6
Line 4
Line 2
Scripps Canyon
Southward dipping beds
Northward dipping beds
Line Locations

Figure 9.

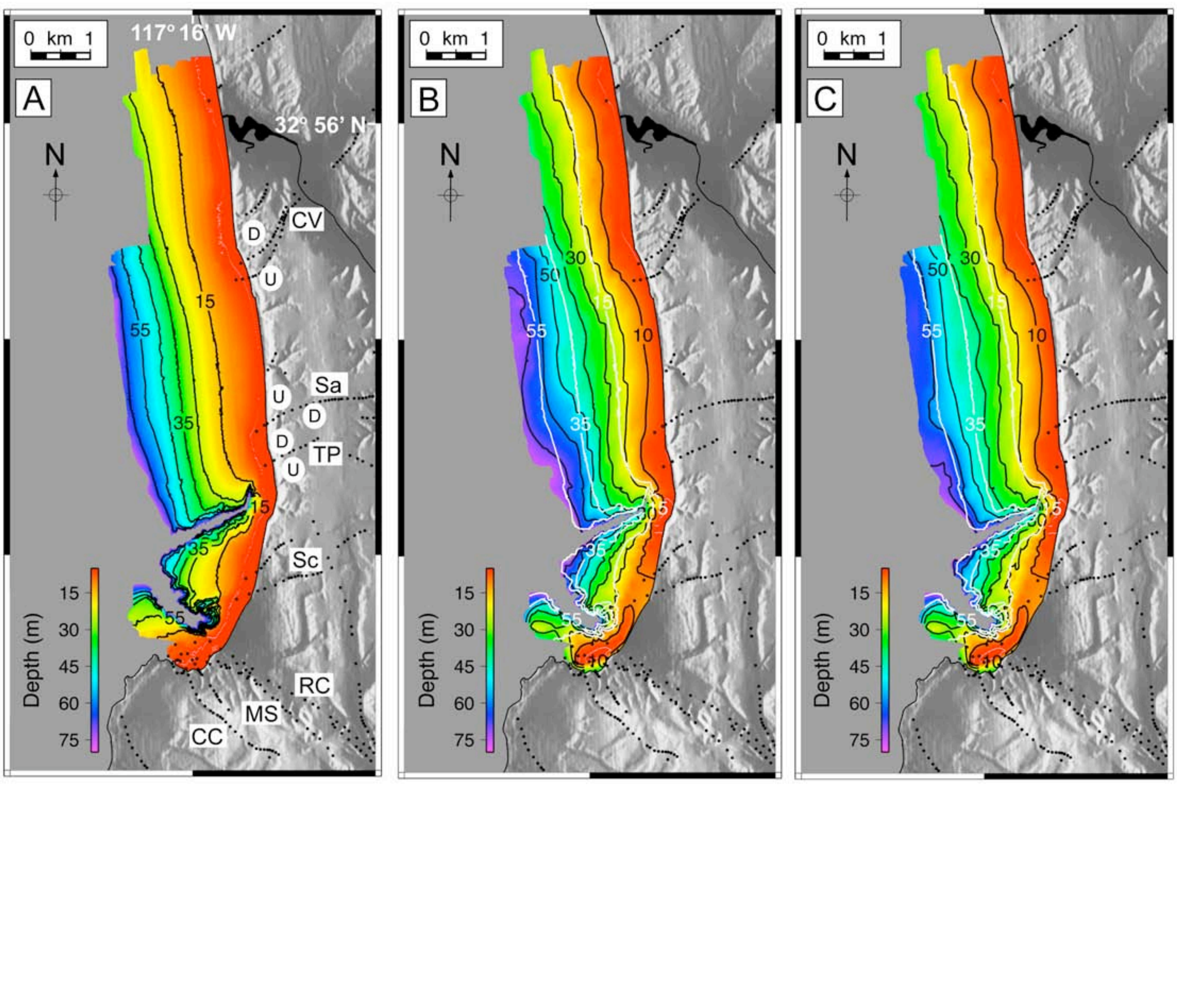

0 km 1
117° 16' W
A
32° 56' N
N
CV
D
U
15
55
Sa
U
D
35
D
TP
U
15
35
Sc
55
Depth (m)
15
30
45
60
75
RC
MS
CC
0 km 1
B
N
50
30
15
10
55
35
10
5
35
55
10
Depth (m)
15
30
45
60
75
0 km 1
C
N
50
30
15
10
55
35
10
5
35
55
10
Depth (m)
15
30
45
60
75

Figure 10.

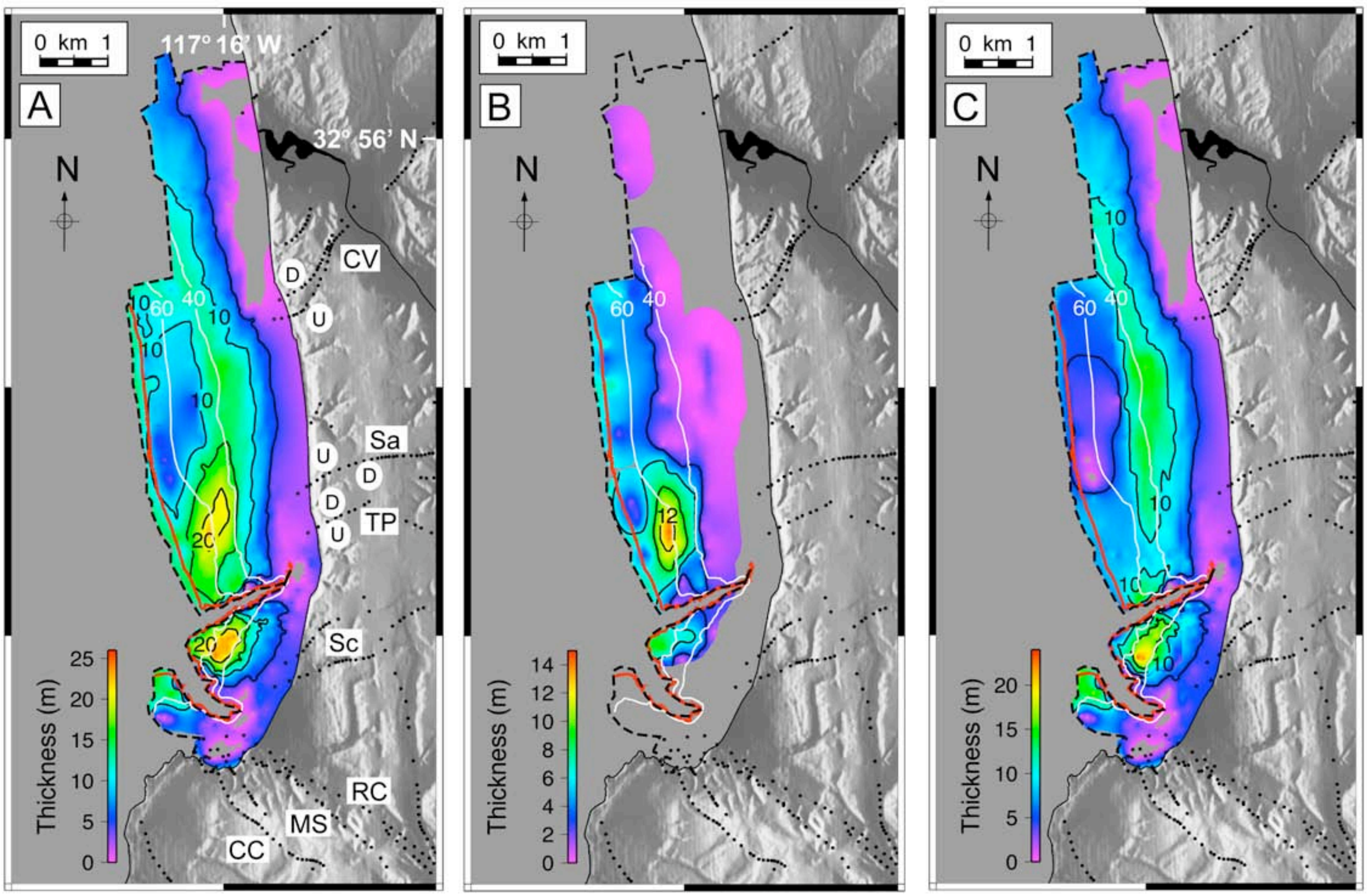
0 km 1
117° 16' W
A
32° 56' N
N
CV
D
U
60
40
10
Sa
TP
20
Sc
RC
MS
CC
Thickness (m)
0
5
10
15
20
25
B
12
14
8
6
4
2
C